INDIAN JOURNAL OF SCIENCE AND TECHNOLOGY

RESEARCH ARTICLE

Polymer nanocomposites comprising PVA matrix and $AgGaO_2$ nanofillers: Probing the effect of intercalation on optical and dielectric response for optoelectronic applications

T E Somesh[1,2], L R Shivakumar[1], M A Sangamesh[3], Siddaramaiah[2], T Demappa[1]*

1 Department of Polymer Science, University of Mysore, India
2 Department of Polymer Science & Technology, JSS Research Foundation, Mysore, India
3 Department of Chemistry, the National Institute of Engineering, Mysore, India

OPEN ACCESS

Received: 29.08.2021
Accepted: 07.09.2021
Published: 22.09.2021

Citation: Somesh TE, Shivakumar LR, Sangamesh MA, Siddaramaiah , Demappa T (2021) Polymer nanocomposites comprising PVA matrix and $AgGaO_2$ nanofillers: Probing the effect of intercalation on optical and dielectric response for optoelectronic applications. Indian Journal of Science and Technology 14(31): 2579-2589. https://doi.org/10.17485/IJST/v14i31.1614

* **Corresponding author**.

tdemappa2003@yahoo.co.in

Funding: None

Competing Interests: None

Published By Indian Society for Education and Environment (iSee)

ISSN
Print: 0974-6846
Electronic: 0974-5645

Abstract

Objectives: Synthesis of hybrid nanoparticles (NPs) and intercalation of as prepared NPs inside polymer matrix to fabricate polymer nanocomposites (NC) and evaluate the optoelectronic properties. **Method:** A simple, time consuming solution combustion method was used to synthesize silver doped gallium oxide ($AgGaO_2$) NPs. The solution casting process was employed to prepare NC films of poly(vinyl alcohol) (PVA) with the inclusion of $AgGaO_2$ NPs as nanofiller. **Finding:** The analytical technique such as Fourier transform infrared spectroscopy, X-ray diffraction, scanning electron microscopy and differential scanning calorimetry analyses were used to analyze the PVA/$AgGaO_2$NC films. The findings of various characterization approaches showed that the morphological, structural and thermal characteristics of PVA/$AgGaO_2$NC films had improved, as well as confirms the existence of $AgGaO_2$ NPs in the PVA matrix. Furthermore, the dielectric characteristics of the PVA/$AgGaO_2$NC films were studied using an LCR meter at various frequencies (50 Hz–1 MHz). With intercalating four different wt% of $AgGaO_2$ NPs content as 0.5, 1, 2 and 4 wt% the dielectric constant and dielectric loss of NC films with 4 wt % $AgGaO_2$NPs incorporated were 112.1 and 51.5 respectively. **Novelty:** This improvement in dielectric characteristics revealed the uniform distribution and effective interaction of $AgGaO_2$ NPs with the active site of PVA chains. The preceding findings demonstrated that the obtained PVA NCs were promising materials for flexible energy storage and UV-shielding applications.

Keywords: Hybrid metal oxides; Dielectric constant and dielectric loss; AC conductivity; Optical energy band gap

1 Introduction

The PNCs have received a lot of interest because of the unusual characteristics that these materials may achieve demonstration great potential applications in the arenas such as energy storage and optoelectronic applications. Polymers can be used as ideal host matrix materials for nanoparticles (NPs) that have exceptional characteristics. In general, adding nanofillers to the polymer matrix modifies the characteristics of the polymer [1–3]. The characteristics of polymer nanocomposites (PNCs) are commonly determined by the particle size, concentration, shape, and dispersion technique of the nanofillers [4,5]. The NPs significantly improve the characteristics of PNCs when compared to pure polymers due to their high surface-to-volume ratio [2]. Poly(vinyl alcohol) (PVA) has been widely utilized as a host polymer for various types of nanofillers among several synthetic polymers. Owed to its simple processability, biocompatibility, great film-forming character, hydrophilicity, excellent chemical resistance, relatively low cost, better aqueous solubility, transmittance, non-toxicity, noncorrosive nature, biodegradability and accessibility with different molecular weights [6]. PVA has high dielectric strength, great charge storage capacity, outstanding mechanical stability, environmental, thermal and chemically stable. PVA has found widespread usage in a variety of applications, including artificial biological devices, electrical devices, a medicinal field for drug delivery systems, textile applications, optoelectronic devices, packaging, layer coating, and filtration applications [7,8]. Moreover, PVA made with a backbone of carbon that contains -OH groups, which can serve as a source of hydrogen bonding contact with the nanofiller and facilitate the production of PVA-based NC. Because of these various benefits, PVA was chosen as the matrix material in the current investigation. PVA was filled with a variety of fillers to improve or change its dielectric [9], optical [10], mechanical [11], and membranes for separation characteristics [12]. $AgGaO_2$ is a broad bandgap semiconductor with bandgap energy of around 1.9 to 2.3 eV at room temperature, whereas Ga_2O_3 has a band gap of ∼4.9 eV [13] which is very high when compare to silver doped. $AgGaO_2$ possesses several good physicochemical characteristics and has prospective applications in a variety of technological fields, including optoelectronics and electroluminescence [14]. $AgGaO_2$ is also used in a variety of other applications [13]. In addition, $AgGaO_2$ NPs were utilized as nanofillers in the production of PNCs. Many techniques exist for producing metal-oxide NPs, including mechanochemical [15], co-precipitation method [16], microwave hydrothermal [17], microwave aided solvothermal [18], sol-gel [19], and chemical precipitation [20]. Many of these approaches entail the use of hazardous chemicals, energy and time consuming also are not cost-effective. As a result, these techniques are unsuitable for industrial-scale NP synthesis. Several researchers have used microbes to produce various metal nanoparticles in order to meet the increasing need for eco-friendly nanoparticles [21]. Agriculture scrap (waste) extracts and plants have recently been used as a reducing agent in the NPs synthesis methods [22], although their potential for the production of metal oxides have to be thoroughly investigated so far because they are time-consuming and scale up the process is highly difficult. Solution combustion synthesis [23,24] is a flexible, simple, and fast technique that enables the efficient synthesis of a wide range of nanomaterials. This method comprises a self-sustaining reaction in a homogenous solution containing several fuel and oxidizers. This method of synthesis enables molecular level mixing, high degree of consistency and due to fast reaction time lower the crystallization temperature and it is simple to regulate the crystallite size and stoichiometric ratios [25]. The solution combustion synthesis approach is a low-temperature process that produces oxides by a distinctive mechanism using a self-ignited exothermic redox reaction. In the present work, the host polymer was an eco-friendly, water-soluble polymer called PVA, and chromium oxide nanoparticles were distributed in the polymer matrix as fillers. The PVA/$AgGaO_2$ nanocomposite films were created using the solution casting technique, with $AgGaO_2$ NPs loading ranging from 0.5 to 4wt% in the PVA matrix. To explore the influence of $AgGaO_2$ NPs on structural, morphological, and thermal characteristics NC films were studied using several analytical methods such as FTIR, XRD, SEM, and DSC. The dielectric characteristics of PVA/$AgGaO_2$ NC films were also investigated.

2 Experimental details

2.1 Materials

Silver nitrate [$AgNO_3$], Gallium nitrate ($Ga(NO_3)_3$), High molecular weight of PVA powder (85,000–124,000 g/mol) and glycine were procured from the supplier Sd-Fine chemicals Pvt. Ltd., India. In the entire synthesis procedure, double distilled water was the solvent in the entire experiments.

2.2 Preparation of $AgGaO_2$ NPs

The solution combustion method was used to prepare nano-sized $AgGaO_2$ [26]. The measured quantities of $AgNO_3$ and $Ga(NO_3)_3$was used as an oxidant were taken in stoichiometric ratios of 1:4 respectively and dissolved in dist. H_2O with continuously magnetically stirred for 30 minutes. The separate solutions were then combined for roughly 1 hour with constant

stirring, and the pH was corrected to 9.5 using 0.1 N NaOH solutions. Drop by drop, glycine (fuel) was added to the aforementioned reaction mixture, and the entire solution (the molar ratio of oxidant to fuel was 1:2) was maintained with steady stirring. After 30 min stirring was continued at 90 °C for 2 hours with continuous stirring, yielding darkish gel material. To make a fine powder, the mixture was heating until it combusted. Finally, the $AgGaO_2$ NPs were produced by calcining the resulting dark greyish powder at 650–800 °C for 2 hours.

The following is a hypothetical chemical reaction:

$$9AgNO_3 + 9GaNO_3 + 20C_2H_5NO_2 \rightarrow 9AgGaO_2 + 40CO_2 \uparrow + 50H_2O + 28\ N_2$$

2.3 Preparation of PVA/$AgGaO_2$ nanocomposite films

The pristine PVA and PVA/$AgGaO_2$NC films with different $AgGaO_2$ NP loadings (0–4 wt%) were made using the solution casting process. By keeping the PVA was dissolved in dist. H_2O at 60 °C for 3 to 4 hours on a magnetic hot plate stirrer with constant stirring. Simultaneously, the $AgGaO_2$ NPs were well dispersed using an ultra-sonicator in dist.H_2O for 30 minutes at room temperature before being mixed with the PVA solution. After completely dissolve with clear PVA solution was then integrated the dispersed NPs slowly and agitated consistently at room temperature. This intricate solution was agitated for about 2 hours, and sonicated for 20 minutes for better dispersion before being placed into a Teflon-lined mould and dried at 60 °C in hot air oven for 4 hours. The PVA/$AgGaO_2$ nanocomposite films that resulted were peeled from the mould and stored in vacuum desiccators before being used for additional characterizations.

2.4 Characterizations

The interaction between the integrated components in NC was evaluated by Fourier-transform infrared (FTIR) spectroscopy, JASCO 4100 spectrometer, Japan. The films were scanned over the wave number range 500–4000cm^{-1}. X-ray diffraction (XRD) analysis of pristine $AgGaO_2$NPs and PNC films was recorded by PROTO AXRDBenchtop powder XRD, Japan, with Cu–Kα radiation(λ = 0.154 nm) source, operated at 40 kV and 40 mA in the 2θrange 10–70° at the scan speed of 0.05°/sec. The morphological behaviors such as structure, topology and roughness of prepared $AgGaO_2$and NCs have been recorded by scanning electron microscope (SEM), JEOL-IT300LV, Japan. The dielectric property and AC conductivity of NC films have been measured by Hioki LCR Meter (AC measurement), Model 3532-50, Switzerland. The dialectical studies have been carried out in the frequency range of 50Hz–5MHz at room temperature. Both the surface of films were circularly coated with silver paste and fixed between the electrodes which have a diameter of 1cm. The thermal characteristics of the NCs have been evaluated using differential scanning calorimetry (DSC), TA Q200, USA. The weight of the sample around 6 mg was scanned at a heating rate of 10°C/min in the temperature range 40–240 °C under nitrogen gas purge. The photonic absorption and transmission characteristics have been established by UV–Visible spectrophotometer, Shimadzu-1800, Japan in the wave length range 200–850 nm.

3 Results and discussions

3.1 FTIR spectroscopy

Figure 1 shows the FTIR spectra of pure PVA and PVA/$AgGaO_2$ nanocomposite films. Spectra show the broadband FTIR spectra of PVA film, which is due to –OH stretching vibration at 3376 cm^{-1}. The stretching vibration of the C–H alkyl group causes the band at 2932 cm^{-1}. The peak at 1729 cm^{-1} corresponds to the stretching of the PVA acetate group's C=O bond. CH_2 symmetric bending is responsible for the band at 1426 cm^{-1}. C–H wagging vibrations could explain the peak at 1372 cm^{-1}. The skeletal vibration of PVA corresponds to the peak at 840 cm^{-1} [27]. The PVA/$AgGaO_2$ nanocomposite films showed similar peaks at 577 and 623 cm^{-1} were also appeared, which could be attributed to the stretching vibration of metal-oxygen bond (Al-O). The dipole–dipole interactions between positive charges of Al and Ag NPs and –OH groups of PVA chains may be responsible for the decrease in stretching vibration intensities [28]. Thus, the FTIR data indicate that $AgGaO_2$ NPs have been successfully integrated into the PVA matrix, and that PVA and $AgGaO_2$ NPs have great compatibility, allowing for the development of homogenous PVA/$AgGaO_2$ nanocomposites.

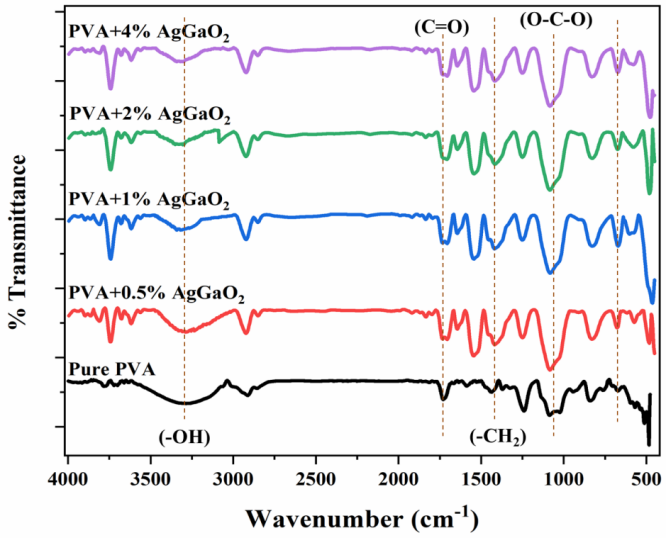

Fig 1. FTIR spectra of pure PVA and PVA/$AgGaO_2$ nanocomposites

3.2 X-ray diffraction analysis

The XRD method was used to investigate the structural identification, quality, and crystallinity of nanocomposite materials. Figure 2a depicts the XRD pattern of $AgGaO_2$ NPs. $AgGaO_2$ nanocrystals have planes at 2θ in 16°, 21°, 28°, 35°, 38°, 44.3°, 64.5°, and 77.4° correspond to lattice planes of (003), (202), (006), (012), (111), (200), (220) and (331) respectively[29]. The average crystallite size (Dp) of the $AgGaO_2$ NPs was estimated using Scherrer's formula $Dp = (K\lambda)/(\beta Cos\theta)$ Where, β = full width at half maximum in radians, θ = Bragg angle, λ = wavelength of incident X-Ray beam and is the constant (k = 0.9). Then the average size was found to be around 24.14 nm. Figure 2b depicts the XRD patterns of pure PVA and PVA/$AgGaO_2$ nanocomposite films loaded with varying weight percentages of $AgGaO_2$ NPs (0–4wt%). The XRD pattern of pure PVA film depicts the semi-crystalline structure of the PVA matrix is demonstrated by the peak at 2θ = 19.9° matching to (101) plane[30]. The very low intensed peak at 2θ 38° corresponding to $AgGaO_2$ NPs appeared in the PVA/$AgGaO_2$ nanocomposites, which might be attributed to NPs gets intercalated inside polymer chains and also very less quantity of NPs in the nanocomposites. The intercalation of the $AgGaO_2$ NPs in the PVA matrix caused a decrease in intensity and moreover small shift in the diffraction peaks of all the PVA/$AgGaO_2$ nanocomposites. The crystallinity of PVA was observed to decrease as the $AgGaO_2$ NPs concentration increased.

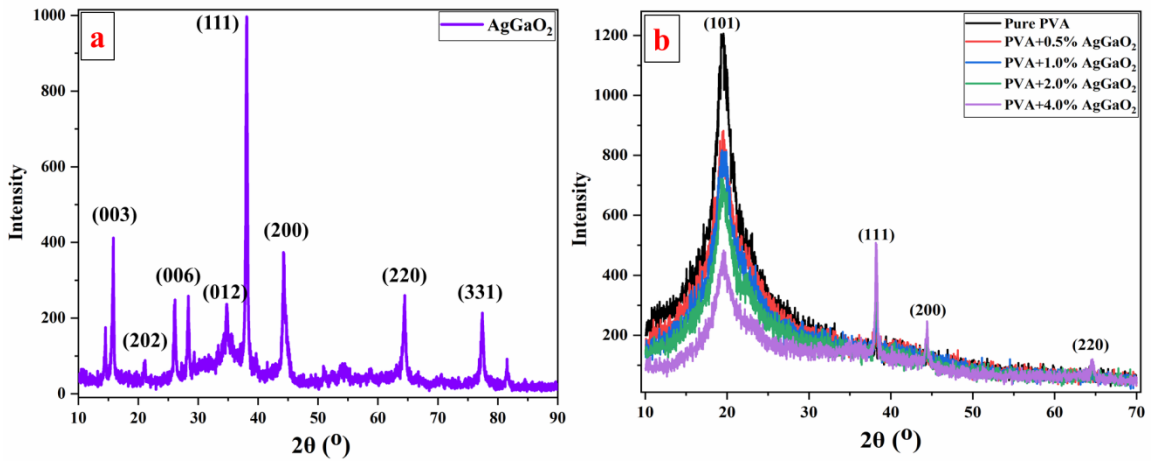

Fig 2. XRD diffractograms of(a) pure $AgGaO_2$ NPs, (b) pure PVA and PVA/$AgGaO_2$ nanocomposites

3.3 Surface morphology

The morphological structure, surface analysis, and influence of dispersion of $AgGaO_2$ NPs in the PVA matrix were investigated using SEM. Figure 3 shows SEM micrographs of pure $AgGaO_2$ NPs and PVA/$AgGaO_2$ nanocomposite films. The solution combustion approach produced crystalline grains and well-structured $AgGaO_2$ NPs, as shown in Figure 3a. SEM micrographs of PVA/$AgGaO_2$ nanocomposite films are shown in Figure 3b-f. The PVA/$AgGaO_2$ nanocomposites surface was found to be relatively rough. The degree of agglomeration was found at increasing with increasing loading levels of $AgGaO_2$ NPs in the PVA matrix. This indicates that $AgGaO_2$ NP dispersion in the PVA matrix was reasonably homogeneous, indicating strong adhesion, interfacial contact, and compatibility between $AgGaO_2$ NPs and the PVA matrix.

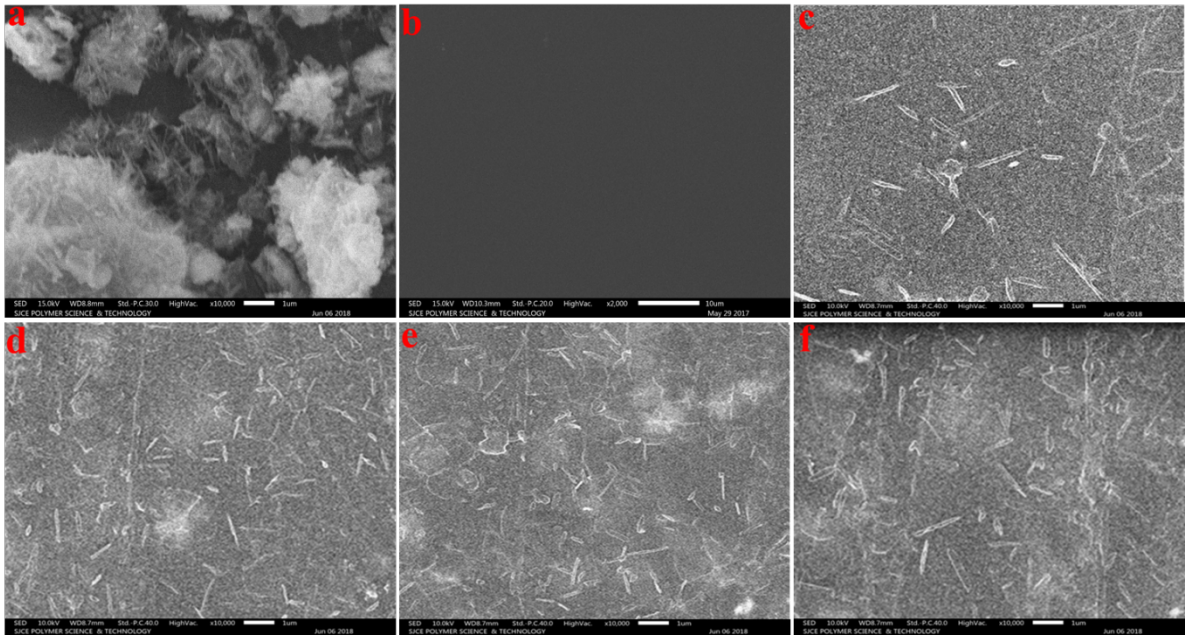

Fig 3. SEM photomicrographs of (a) $AgGaO_2$, (b) pure PVA and PVA/$AgGaO_2$ nanocomposites of (c)0.5, (d) 1, (e) 2 and (f) 4 wt% loaded

3.4 Thermal analysis

DSC thermograms were used to evaluate the thermal properties of PVA/$AgGaO_2$ nanocomposite films in order to determine phase transitions such as glass transition (Tg) and melting (Tm) temperatures. Tg denotes the amorphous phase, while Tm denotes the crystalline properties of PVA. The DSC thermograms of PVA and PVA integrated with 0.5, 1, 2 and 4wt% $AgGaO_2$ are shown in Figure 4. Pure PVA thermograms show Tm and Tg at 192 and 74 degrees Celsius, respectively. As normal, the hydrophilic character of PVA indicated by the large and deep endothermic peak between 100–140°C, to the release of water molecules whose adsorption between the segments of PVA, was absent because the analysis done by the method heat cool heat. Furthermore, the thermograms of PVA/$AgGaO_2$ with varying concentrations of $AgGaO_2$ showed modifications in the thermal characteristics of nanocomposite films. Tg for all nanocomposite films was reduced from 74°C to 72, 71, and 70°C, whereas Tm changed from 192 to 180°C. The ability of crystalline re-ordering of polymer chains was limited by interactions between metal oxides and –OH groups of PVA chains and the larger metaloxide NPs[31]. This occurrence implies that the nanofillers have a negative impact on the crystallinity of the PVA matrix, increasing the amorphous component of the nanocomposite films, making them more flexible. A similar observation has been made elsewhere[32].

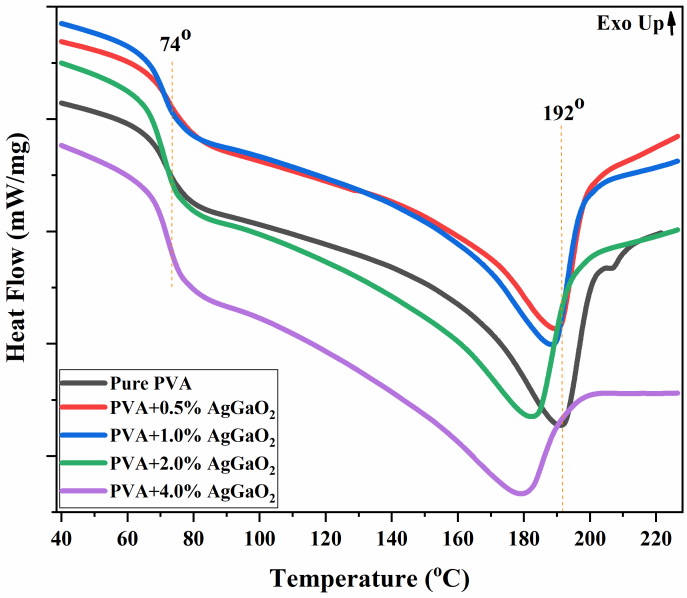

Fig 4. DSC thermograms of pure PVA and PVA/$AgGaO_2$ nanocomposites.

3.5 Electrical properties

The capacity of a substance to retain electrical charges may be assessed via dielectric measurements. Figure 5a shows dielectric constant (ε') graphs of PVA and PVA/$AgGaO_2$ nanocomposite films across a frequency range of 50 Hz to 5MHz. It can be said that the dispersion of $AgGaO_2$ NPs in the PVA matrix results in an increased dielectric constant as well as better electrical characteristics, most likely due to the significant contribution from interfacial polarisation caused by the build-up of trapped charges at the interface [33]. Due to the deposition of space charges at the interfaces, the enhancement in dielectric constant could be produced by the condensed pinning effect of defects on the domain wall motion. As a result, a low excitation electric field can only induce domain wall movement, and the dielectric constant is virtually unaffected by the electric field. Furthermore, these findings confirmed that the composite interfaces have a key role in improving the dielectric characteristics. Furthermore, interfacial polarisation demonstrates that NPs are distributed uniformly throughout the polymer matrix [34]. As a result, an increase in the dielectric constant greatly promotes the improvement in $AgGaO_2$ NP dispersion inside the PVA matrix. Because of differences in interactions among composite components and complexation among them, heterogeneous changes in the dielectric constant were observed when the $AgGaO_2$ content increased. Furthermore, it was found that the dielectric constant values are only high at lower frequencies, possibly due to the presence of interfacial polarisation. Interfacial polarisation can only exist at low frequencies, and as frequency increases, it decreases [35]. The polar molecule rotational motion of the material may not be fast enough to achieve equilibrium with an applied electric field when the frequencies are high [36]. When a result, as the frequency rises, the dielectric constant decreases. Another important feature of dielectric materials is dielectric loss, which is used to assess how much heat energy is dissipated in that material. Figure 5b shows the dielectric loss (ε") plots of the PVA/$AgGaO_2$ nanocomposite films. Higher dielectric loss values were observed at lower frequencies, which could be related to the Maxwell–Wagner effect resulting from charge carrier immigration at the interface or sensitive mobile ionic impurities and polar radicals with dipole moments [37]. The ε" values are low at higher frequencies, which can be attributed to orientation polarisation, which occurs when the polymer chain motion cannot continue inside the phase of a quickly moving applied electric field [37]. Furthermore, as the amount of $AgGaO_2$ NPs in the PVA matrix increased, the dielectric loss increased. In general, the addition of nanofillers increases the charge carriers of a system, resulting in an increase in the ε" of a nanocomposite material. The highest nanofiller concentration resulted in the most effective contact between nanofiller and polymer matrix, resulting in enhanced interfacial or space charge polarisation and hence a higher value of ε". The values of ε' and ε" of PVA/$AgGaO_2$ nanocomposite films are summarised in Table 1.

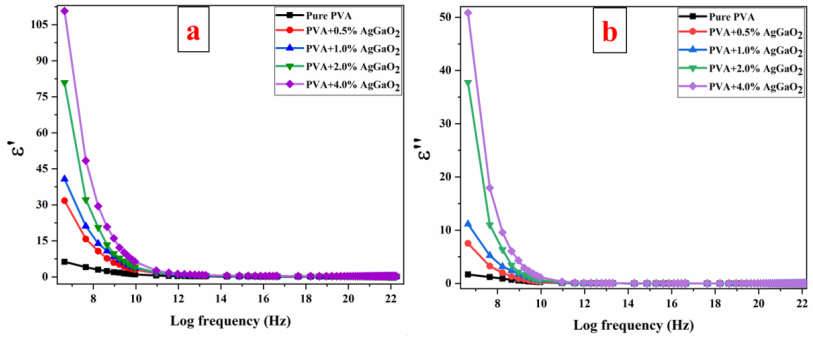

Fig 5. Dielectric constant (a) and dielectric loss (b) as a function of log frequency for pure PVA and PVA/$AgGaO_2$ nanocomposites.

Table 1. Electrical characteristics of pure PVA and PVA/$AgGaO_2$ NC films.

Samples	ε' (logω at 6 Hz)	ε" (logω at 6 Hz)	σ_{ac}(logω at 6 Hz)
Pure PVA	112.1	51.5	8.2×10^{-7}
PVA+0.5% $AgGaO_2$	89.8	37.9	1.3×10^{-6}
PVA+1.0% $AgGaO_2$	42.3	11.9	1.7×10^{-6}
PVA+2.0% $AgGaO_2$	33.2	8.1	2.4×10^{-6}
PVA+4.0% $AgGaO_2$	6.2	1.5	2.9×10^{-6}

Figure 6 shows the AC conductivity (σ_{ac}) of PVA/$AgGaO_2$ as a function of frequency at room temperature. The frequency-dependent conductivity graphs executing two distinguish plateau at low frequencies and at higher frequencies. All NC films have lower ac values at lower frequencies (log 5–13 Hz), and the frequency response of σ_{ac} is minimal. It's due to interfacial resistance and the electrode polarisation effect, in which the tendency for charges to accumulate at the electrode-electrolyte interface leads to a decrease in the number of mobile ions and, as a result, a decrease in ionic conductivity[38]. The σ_{ac} is particularly sensitive and exhibits greater values at higher frequencies, known as hopping frequencies, and attained its ideal value at log 21 Hz, due to long-range movement of charge carriers reaction to applied electric field, and the NC films demonstrate a bulk relaxation phenomenon[39]. Due to an increase in ion route shown in the PVA matrix, which delivers more charge carriers in NC films, the inclusion of $AgGaO_2$ NPs results in the maximum ionic conductivity[40]. In addition, the reduction in the crystallinity of base polymer is credited with the improvement in conductivity. As a result, the great amplitude of the polymer segmental motion aids ionic transport across the PVA/$AgGaO_2$ films matrix[41].

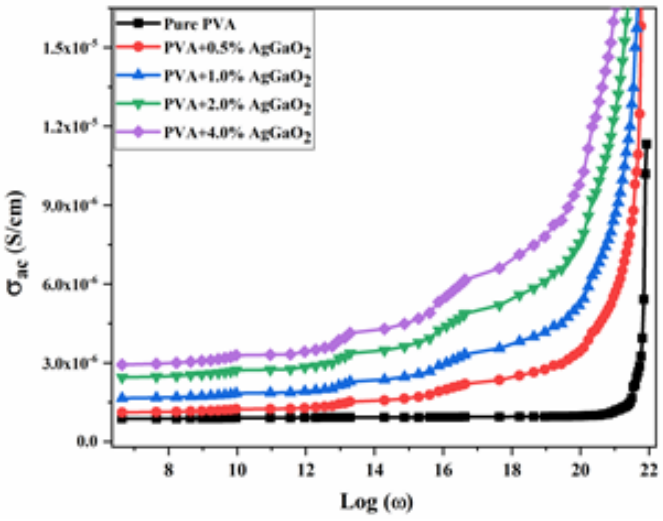

Fig 6. AC Conductivity plot as a function of log frequency of pure PVA and PVA/$AgGaO_2$ nanocomposites.

3.6 Optical studies

3.6.1 Absorption and absorption coefficient

When a photon is absorbed by a material, the transition occurs in the band gap area. The absorption process is shown in plots as an absorption edge, from which the optical band gap energies will be evaluated. The absorption characteristics of PVA and its NC films are shown in Figure 7(a), different electronic transitions may occur in PVA. The absorption band at 230–250 nm is due to an unsaturated C=O of left over acetate groups in the structure of PVA and C=C existing in the polymer chains tail head [6]. Pristine PVA has one more absorption peak at 260–320 nm, which is noticeable, n→π^*inter band transitions of oxygen atoms free electrons in polymer chains are ascribed to these peaks [42]. Figure 7(a) shows that with increasing $AgGaO_2$ content in NC films, both the absorption bands are somewhat merged, accompanied with an upsurge the intensity of absorption peaks. The influence of $AgGaO_2$ contents is revealed by a considerable change in the absorbance profile and a redshift in the UV frequency band. After 450 nm, there is a broad noticeable band on the absorption spectra of higher concentration loading NC films; this may be attributed to the silver particles present in the $AgGaO_2$NPs. Where the absorption was lowered and come to be constant at higher wavelengths due to the lower energy of incident light. The absorption coefficient (α), which can be evaluated using absorbance (A) using Beer Lambert's law (α = (2.303/d)*A), is an important parameter to describe the nature of the optical transition of the NC films. Figure 7(b) shows plots of α versus photon energy (hυ) for PVA/$AgGaO_2$NC films with varied quantities of NP. With increasing NP concentration, the absorption edge for PVA/$AgGaO_2$was shown to increase. This is due to the NPs intercalated were active and get absorb the photon energy also the increased degree of amorphous nature of PVA/$AgGaO_2$ as a result the mobility of polymer chain increases and polar groups become active. The absorption coefficient is the rate at which light intensity decreases compared to its propagation path. It's a property of a material that determines how much light it absorbs.

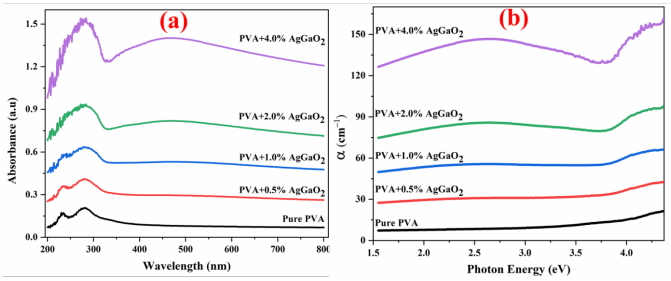

Fig 7. (a) Absorbance as a function of wavelength and (b) absorption coefficient as a function of photon energy for pure PVA and PVA/$AgGaO_2$ nanocomposites.

3.6.2 Tauc's Plots

Figure 8 (a,b), shows plots of direct and indirect band gap energy that were plotted against photon energy and in Table 2 the resulting values were tabulated. The direct band gap energy of PVA is 4.82 eV, while doped PVA films have values ranging from 3.64 to 2.73 eV. It was revealed that as the $AgGaO_2$ content increases, band gap energy drops, possibly due to formation of charge-transfer complex and an increase in the degree of disorder. As the amorphous character of NC films increases, it leads to an increase of mobile charge carriers [43]. The results found from XRD profiles backs up these findings.

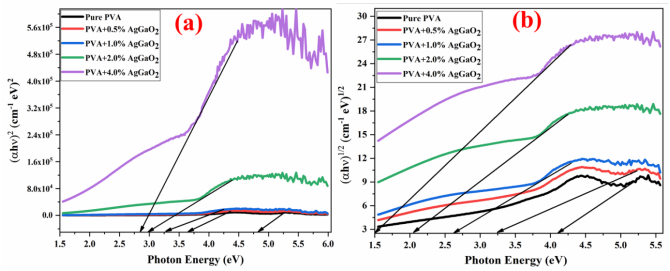

Fig 8. (a) Direct and (b) Indirect Tauc's plots as a function of photon energy for pristine PVA and PVA/$AgGaO_2$ nanocomposites.

3.6.3 Refractive index and optical conductivity

Optical properties like refractive index (n) and optical conductivity (opt) are critical when choosing materials for a certain optoelectronic application. The Figure 9 shows the n of PVA/$AgGaO_2$ NC films plotted against wavelength. Using eq. (1), then maybe calculated using the reflectance (R) and optical extinction values as follows:

$$n = \frac{1+\sqrt{R}}{1-\sqrt{K}}$$

Where K is the extinction coefficient, the optimum values of n for pure PVA, which reveals where the polymer absorbs incident light at absorption maxima of 232 and 280 nm, can be seen at lower wavelengths. Then, when the wavelength increases up to 600 nm, the n values decrease, and as the wavelength increases further, there are no substantial changes, and n tends to be constant. Table 2 summarises the n values observed for all NC films. Furthermore, as the amount of $AgGaO_2$ in the NC films increases, then increases dramatically. It could be associated with increases in the polarizability of NC films, where n corresponds to the polarisation of molecules generated by electromagnetic fields[44]. Polarized molecules will interact with incident light, and these molecules will have a greater tendency to decrease the speed of light passing through the PVA chains. The existence of $AgGaO_2$ NPs, there will be more electrons density and polarizable molecules, resulting in a higher n value according to the Lorentz-Lorenz principle[45].

The σ_{opt} can be calculated from the equation $\sigma_{opt}=\alpha nc/4\pi$ where,c is the velocity of light, n is the refractive index andα is the absorption coefficient. σ_{opt} is a useful method for determining the electronic states of materials. The term "optical conductivity" refers to the conductivity those results from optical excitation without the electrostatic force[46]. The σ_{opt} versus wavelength is shown in Figure 9(b). When $AgGaO_2$ was added to PVA, the optical conductivity of the PVA NC increased. The generation of CTC between $AgGaO_2$ and PVA chains can be interpreted. As a result, the increase in optical conductivity of NC films caused by the addition of $AgGaO_2$ can be ascribed to an upsurge in charge carrier mobility, which varies depending on the $AgGaO_2$ content. Higher photon energy enhances optical conductivity, which could be owing to electron excitation caused by absorbing photon energy, as well as the high absorbance of NC films in that region[47]. As a result of the decrease in the energy band gap of PVA/$AgGaO_2$ NC films, the σ_{opt} increases from 9.1×10^9 to $2\times10^{11}S^{-1}$ as the EC concentration increases.

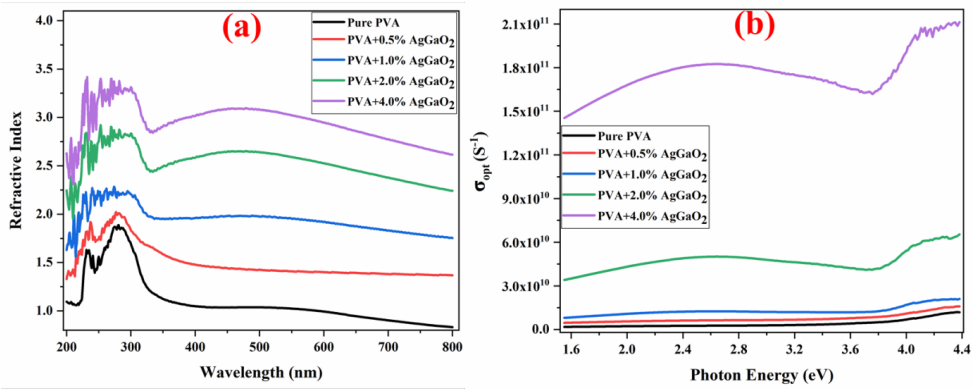

Fig 9. (a) Refractive index as a function of wavelength and (b) optical conductivity as a function of photon energy for pure PVA and PVA/$AgGaO_2$ nanocomposites.

Table 2. Optical characteristics of pristine PVA and PVA/$AgGaO_2$ NC films

Samples	α (cm^{-1})	$(\alpha h\upsilon)^2$ (cm^{-1} eV)^2	$(\alpha h\upsilon)^{1/2}$ (cm^{-1} eV)$^{1/2}$	n	$\sigma_{opt}\times10^{10}$ (S^{-1})
Pure PVA	21.59	4.82	4.08	1.08	0.91
PVA+0.5% $AgGaO_2$	43.29	3.64	3.23	1.37	1.70
PVA+1.0% $AgGaO_2$	66.57	3.28	2.61	1.69	2.30
PVA+2.0% $AgGaO_2$	98.46	2.98	2.06	2.13	6.78
PVA+4.0% $AgGaO_2$	162.30	2.73	1.51	2.51	20.08

4 Conclusions

$AgGaO_2$ NPs were prepared to employ a time and energy-consuming simple technique with self-igniting solution combustion method. As-prepared $AgGaO_2$ NP was successfully incorporated into a polymer chain utilizing a simple and environmental friendly solution casting process to fabrication of PVA/$AgGaO_2$ nanocomposite films. XRD, FTIR, SEM, and DSC methods were used to examine the thermal, morphological, and structural properties of these nanocomposites. The $AgGaO_2$ NPs and the PVA matrix showed strong interactions and great compatibility in the XRD and FTIR measurements. The uniform dispersion of $AgGaO_2$ NPs inside the PVA matrix was confirmed by SEM investigations. The DSC results showed that PVA/$AgGaO_2$ nanocomposites have decreased the crystallinity than pure PVA, which helps to increase the mobile charge carriers inside polymer. Finally, better dielectric properties resulted from the uniform distribution and integration of $AgGaO_2$ NPs within the PVA matrix, which could be useful in energy storage devices.

References

1) Xie X, Yang C, dong Qi X, hui Yang J, wan Zhou Z, Wang Y. Constructing polymeric interlayer with dual effects toward high dielectric constant and low dielectric loss. *Chemical Engineering Journal*. 2019;366:378–389. Available from: https://dx.doi.org/10.1016/j.cej.2019.02.106.
2) Subramani NK, Nagaraj SK, Shivanna S, Siddaramaiah H. Highly Flexible and Visibly Transparent Poly(vinyl alcohol)/Calcium Zincate Nanocomposite Films for UVA Shielding Applications As Assessed by Novel Ultraviolet Photon Induced Fluorescence Quenching. *Macromolecules*. 2016;49(7):2791–2801. Available from: https://dx.doi.org/10.1021/acs.macromol.5b02282.
3) Gong X, Tang CY, Pan L, Hao Z, Tsui CP. Characterization of poly(vinyl alcohol) (PVA)/ZnO nanocomposites prepared by a one-pot method. *Composites Part B: Engineering*. 2014;60:144–149. Available from: https://dx.doi.org/10.1016/j.compositesb.2013.12.045.
4) Thabet A, Ebnalwaled AA. Improvement of surface energy properties of PVC nanocomposites for enhancing electrical applications. *Measurement*. 2017;110:78–83. Available from: https://dx.doi.org/10.1016/j.measurement.2017.06.023.
5) Muzaffar A, Ahamed MB, Deshmukh K, Faisal M, Pasha SKK. Enhanced electromagnetic absorption in NiO and BaTiO3 based polyvinylidenefluoride nanocomposites. *Materials Letters*. 2018;218:217–220. Available from: https://dx.doi.org/10.1016/j.matlet.2018.02.029.
6) Somesh TE, Al-Gunaid MQA, Madhukar BS, Siddaramaiah. Photosensitization of optical band gap modified polyvinyl alcohol films with hybrid AgAlO2 nanoparticles. *Journal of Materials Science: Materials in Electronics*. 2019;30(1):37–49. Available from: https://dx.doi.org/10.1007/s10854-018-0226-3.
7) Al-Gunaid MQA, Saeed AMN, Subramani NK, Madhukar BS, Siddaramaiah. Optical parameters, electrical permittivity and I–V characteristics of PVA/Cs2CuO2 nanocomposite films for opto-electronic applications. *Journal of Materials Science: Materials in Electronics*. 2017;28(11):8074–8086. Available from: https://dx.doi.org/10.1007/s10854-017-6513-6.
8) Dhatarwal P, Sengwa RJ. Investigation on the optical properties of (PVP/PVA)/Al2O3 nanocomposite films for green disposable optoelectronics. *Physica B: Condensed Matter*. 2021;613(15):412989. Available from: https://dx.doi.org/10.1016/j.physb.2021.412989.
9) Rani P, Ahamed MB, Deshmukh K. Structural, dielectric and EMI shielding properties of polyvinyl alcohol/chitosan blend nanocomposites integrated with graphite oxide and nickel oxide nanofillers. *Journal of Materials Science: Materials in Electronics*. 2021;32(1):764–779. Available from: https://dx.doi.org/10.1007/s10854-020-04855-w.
10) Sheha E, Khoder H, Shanap TS, El-Shaarawy MG, Mansy MKE. Structure, dielectric and optical properties of p-type (PVA/CuI) nanocomposite polymer electrolyte for photovoltaic cells. *Optik*. 2012;123(13):1161–1166. Available from: https://dx.doi.org/10.1016/j.ijleo.2011.06.066.
11) Somalika P, Santoshkumar S, Jitendra P. Badgayan Nitesh Dhar. An insight into mechanical & thermal properties of shape memory polymer reinforced with nanofillers; a critical review. *Materials Today: Proceedings*. 2021. Available from: https://doi.org/10.1016/j.matpr.2021.07.504.
12) Huang Z, Yang G, Zhang J, Gray S, Xie Z. Dual-layer membranes with a thin film hydrophilic MOF/PVA nanocomposite for enhanced antiwetting property in membrane distillation. *Desalination*. 2021;518:115268. Available from: https://dx.doi.org/10.1016/j.desal.2021.115268.
13) Zade VB, Rajkumar MR, Broner R, Ramana CV. Chemical composition tuning induced variable and enhanced dielectric properties of polycrystalline Ga 2-2 x W x O 3 ceramics. *Engineering Reports*. 2021;3(1):e12300. doi:10.1002/eng2.12300.
14) Manzoor K, Vadera SR, Kumar N, Kutty TRN. Multicolor electroluminescent devices using doped ZnS nanocrystals. *Applied Physics Letters*. 2004;84(2):284–286. Available from: https://dx.doi.org/10.1063/1.1639935.
15) Pathak CS, Mandal MK, Agarwala V. Synthesis and characterization of zinc sulphide nanoparticles prepared by mechanochemical route. *Superlattices and Microstructures*. 2013;58:135–143. Available from: https://dx.doi.org/10.1016/j.spmi.2013.03.011.
16) Salama AH, Youssef AM, Rammah YS, El-Khatib M. YBCO as a transition metal oxide ceramic material for energy storage. *Bulletin of the National Research Centre*. 2019;43(1):1–1. Available from: https://dx.doi.org/10.1186/s42269-019-0134-6.
17) Yin L, Wang D, Huang J, Cao L, Ouyang H, Yong X. Morphology-controllable synthesis and enhanced photocatalytic activity of ZnS nanoparticles. *Journal of Alloys and Compounds*. 2016;664:476–480. Available from: https://dx.doi.org/10.1016/j.jallcom.2015.10.281.
18) Porta FAL, Ferrer MM, de Santana YVB, Raubach CW, Longo VM, Sambrano JR, et al. Synthesis of wurtzite ZnS nanoparticles using the microwave assisted solvothermal method. *Journal of Alloys and Compounds*. 2013;556:153–159. Available from: https://dx.doi.org/10.1016/j.jallcom.2012.12.081.
19) Ahsan HM, Lal K, Saleem M, Mustafa GM, Khan MA, Haidyrah AS, et al. Tuning the dielectric behavior and energy storage properties of Mn/Co co-doped ZnO. *Materials Science in Semiconductor Processing*. 2021;134:105977. Available from: https://dx.doi.org/10.1016/j.mssp.2021.105977.
20) Chandrasekar LB, Chandramohan R, Vijayalakshmi R, Chandrasekaran S. Preparation and characterization of Mn-doped ZnS nanoparticles. *International Nano Letters*. 2015;5(2):71–75. Available from: https://dx.doi.org/10.1007/s40089-015-0139-6.
21) Prasad K, Jha AK. Biosynthesis of CdS nanoparticles: An improved green and rapid procedure. *Journal of Colloid and Interface Science*. 2010;342(1):68–72. Available from: https://dx.doi.org/10.1016/j.jcis.2009.10.003.
22) Pasha K, Lakshmipathy R, Sarada NC, Chidambaram K. One-step, low-temperature fabrication of CdS quantum dots by watermelon rind: a green approach. *International Journal of Nanomedicine*. 2015;10(1):183. Available from: https://dx.doi.org/10.2147/ijn.s79988.
23) Reddy AJ, Kokila MK, Nagabhushana H, Rao JL, Shivakumara C, Nagabhushana BM, et al. Combustion synthesis, characterization and Raman studies of ZnO nanopowders. *Spectrochimica Acta Part A: Molecular and Biomolecular Spectroscopy*. 2011;81(1):53–58. Available from: https://dx.doi.org/10.1016/j.saa.2011.05.043.

24) Deganello F, Tyagi AK. Solution combustion synthesis, energy and environment: Best parameters for better materials. *Progress in Crystal Growth and Characterization of Materials*. 2018;64:23–61. Available from: https://dx.doi.org/10.1016/j.pcrysgrow.2018.03.001.
25) Aruna ST, Mukasyan AS. Combustion synthesis and nanomaterials. *Current Opinion in Solid State and Materials Science*. 2008;12:44–50. Available from: https://dx.doi.org/10.1016/j.cossms.2008.12.002.
26) Al-Gunaid MQA, E ST, M GH, Al-Ostoot FH, Basavarajaiah S. Optimized nano-perovskite lanthanum cuprate decorated PVA based solid polymer electrolyte. *Polymer-Plastics Technology and Materials*. 2020;59:215–229. Available from: https://dx.doi.org/10.1080/25740881.2019.1634729.
27) Nguyen TP, Le AD, Vu TB, Lam QV. Investigations on photoluminescence enhancement of poly(vinyl alcohol)-encapsulated Mn-doped ZnS quantum dots. *Journal of Luminescence*. 2017;192:166–172. Available from: https://dx.doi.org/10.1016/j.jlumin.2017.06.031.
28) Chandrakala HN, Ramaraj B, Shivakumaraiah, Madhu GM, Siddaramaiah. Preparation of Polyvinyl Alcohol–Lithium Zirconate Nanocomposite Films and Analysis of Transmission, Absorption, Emission Features, and Electrical Properties. *The Journal of Physical Chemistry C*. 2013;117(9):4771–4781. Available from: https://dx.doi.org/10.1021/jp311828n.
29) Ouyang S, Kikugawa N, Chen D, Zou Z, Ye J. A Systematical Study on Photocatalytic Properties of AgMO2 (M = Al, Ga, In): Effects of Chemical Compositions, Crystal Structures, and Electronic Structures. *The Journal of Physical Chemistry C*. 2009;113(4):1560–1566. Available from: https://dx.doi.org/10.1021/jp806513t.
30) Friedlander HN, Harris HE, Pritchard JG. Structure–property relationships of poly(vinyl alcohol). I. Influence of polymerization solvents and temperature on the structure and properties of poly(vinyl alcohol) derived from poly(vinyl acetate). *Journal of Polymer Science Part A-1: Polymer Chemistry*. 1966;4(3):649–664. Available from: https://dx.doi.org/10.1002/pol.1966.150040319.
31) Samir MASA, Alloin F, Gorecki W, Sanchez JY, Dufresne A. Nanocomposite Polymer Electrolytes Based on Poly(oxyethylene) and Cellulose Nanocrystals. *The Journal of Physical Chemistry B*. 2004;108(30):10845–10852. Available from: https://dx.doi.org/10.1021/jp0494483.
32) Chiodelli G, Ferloni P, Magistris A, Sanesim. Ionic conduction and thermal properties of poly (ethylene oxide)-lithium tetrafluoroborate films. *Solid State Ionics*. 1988;(90321):28–30. doi:10.1016/0167-2738(88)90321-9.
33) Varaprasad HS, Sridevi PV, Anuradha MS. Optical, morphological, electrical properties of ZnO-TiO2-SnO2/CeO2 semiconducting ternary nanocomposite. *Advanced Powder Technology*. 2021;32:1472–1480. Available from: https://dx.doi.org/10.1016/j.apt.2021.02.042.
34) Tantis I, Psarras GC, Tasis D. Functionalized graphene – poly(vinyl alcohol) nanocomposites: Physical and dielectric properties. *Express Polymer Letters*. 2012;6:283–292. Available from: https://dx.doi.org/10.3144/expresspolymlett.2012.31.
35) Murugaraj P, Mainwaring D, Mora-Huertas N. Dielectric enhancement in polymer-nanoparticle composites through interphase polarizability. *Journal of Applied Physics*. 2005;98(5):054304. Available from: https://dx.doi.org/10.1063/1.2034654.
36) Kamath A, Devendrappa H. Concentration-dependent ionic conductivity and dielectric relaxation of methyl blue-dyed polyethylene oxide films. *Polymer Bulletin*. 2015;72(10):2705–2724. Available from: https://dx.doi.org/10.1007/s00289-015-1431-3.
37) Akhtar AN, Murtaza G, Shafique MA, Haidyrah AS. Effect of Cu Ions Implantation on Structural, Electronic, Optical and Dielectric Properties of Polymethyl Methacrylate (PMMA). *Polymers*. 2021;13(6):973–973. Available from: https://dx.doi.org/10.3390/polym13060973.
38) Venkateswarlu M, Knarasimha R, Rambabu B, Satyanarayana N. A.c. conductivity and dielectric studies of silver-based fast ion conducting glass system. *Solid State Ionics*. 2000;127(1-2):177–184. doi:10.1016/S0167-2738(99)00257-X.
39) Radoń A, Hawełek Ł, Łukowiec D, Kubacki J, Włodarczyk P. Dielectric and electromagnetic interference shielding properties of high entropy (Zn,Fe,Ni,Mg,Cd)Fe2O4 ferrite. *Scientific Reports*. 2019;9(1):1–3. Available from: https://dx.doi.org/10.1038/s41598-019-56586-6.
40) Huan CHW, Chuhyung W, Chein HC, Yao-Hui. The effect of different lithium salts on conductivity of comb-like polymer electrolyte with chelating functional group. *Electrochimica acta*. 2003;48:679–690. doi:10.1016/S0013-4686(02)00737-5.
41) Ravi M, Pavani Y, Kumar KK, Bhavani S, Sharma AK, Rao VVRN. Studies on electrical and dielectric properties of PVP:KBrO4 complexed polymer electrolyte films. *Materials Chemistry and Physics*. 2011;130(1-2):442–448. Available from: https://dx.doi.org/10.1016/j.matchemphys.2011.07.006.
42) Ibrahim S, Ahmad R, Johan MR. Conductivity and optical studies of plasticized solid polymer electrolytes doped with carbon nanotube. *Journal of Luminescence*. 2012;132(1):147–152. Available from: https://dx.doi.org/10.1016/j.jlumin.2011.08.004.
43) Praveena SD, Ravindrachary V, Ismayil RFB. Dopant-induced microstructural, optical, and electrical properties of TiO2 /PVA composite. *Polymer Composites*. 2016;37(4):987–997. doi:10.1002/pc.23258.
44) An N, Zhuang B, Li M, Lu Y, Wang ZG. Combined Theoretical and Experimental Study of Refractive Indices of Water–Acetonitrile–Salt Systems. *The Journal of Physical Chemistry B*. 2015;119(33):10701–10709. Available from: https://dx.doi.org/10.1021/acs.jpcb.5b05433.
45) Khalil KD, Bashal AH, Khalafalla M, Zaki AA. Synthesis, structural, dielectric and optical properties of chitosan-MgO nanocomposite. *Journal of Taibah University for Science*. 2020;14(1):975–983. Available from: https://dx.doi.org/10.1080/16583655.2020.1792117.
46) Saeed AMN, Hezam A, Al-Gunaid MQA, E ST, Siddaramaiah. Effect of ethylene carbonate on properties of PVP-CsAlO2-LiClO4 solid polymer electrolytes. *Polymer-Plastics Technology and Materials*. 2021;60:132–146. Available from: https://dx.doi.org/10.1080/25740881.2020.1793191.
47) Farag AAM, Yahia IS. Structural, absorption and optical dispersion characteristics of rhodamine B thin films prepared by drop casting technique. *Optics Communications*. 2010;283(21):4310–4317. Available from: https://dx.doi.org/10.1016/j.optcom.2010.06.081.